# Effects of Alkylation on Deviations from Lennard−Jones Collision Rates for Highly Excited Aromatic Molecules: Collisions of Methylated Pyridines with HOD†

**Qingnan Liu, Daniel K. Havey, Ziman Li, and Amy S. Mullin***

*Department of Chemistry and Biochemistry, University of Maryland College Park, Maryland 20705*

*Received: December 15, 2008; Revised Manuscript Received: January 28, 2009*

Collision rates and energy transfer distributions are reported for HOD with highly vibrationally excited 2-methylpyridine (2-picoline, $E = 38\,310$ cm$^{-1}$) and 2,6-dimethylpyridine (2,6-lutidine, $E = 38\,700$ cm$^{-1}$). High resolution transient IR absorption is used measured to complete product state distributions of scattered HOD(000) molecules with $E_{rot} = 109$ to 1331 cm$^{-1}$. Doppler-broadened line profiles characterize the depletion and appearance for HOD molecules due to collisions with hot donors and show that the product translational and rotational energy distributions are similar for both donors with $\langle \Delta E_{rel} \rangle = 370$ cm$^{-1}$ and $\langle \Delta E_{rot} \rangle \sim 75$ cm$^{-1}$. The energy transfer rate for picoline (E)/HOD is 2.5 times larger than the Lennard−Jones collision rate. The energy transfer rate for lutidine(E)/HOD is 3.2 times larger than the Lennard−Jones collision rate. Previous work (Havey, Liu, Li, Elioff, and Mullin, *J. Phys. Chem. A* **2007**, *111*, 13321−9) reported similar energy transfer values for pyrazine/HOD collisions and an energy transfer rate that is 1.7 times the Lennard−Jones collision rate. The observed collision rates are discussed in terms of hydrogen bonding interactions between HOD and the aromatic donor molecules. Energy gain profiles for HOD are compared with those for $H_2O$.

## Introduction

Water is a primary product of hydrocarbon combustion and is ubiquitous in the earth's atmosphere. The means by which water quenches highly excited molecules has important implications in many practical settings. Quenching collisions can deactivate highly excited molecules by removing energy that is needed for reaction and such collisions compete directly with unimolecular decomposition and activated bimolecular reactions.[1−3] State-resolved product distributions have been measured previously for $H_2O$ that are scattered in high rotational states ($E_{rot} >$ 1000 cm$^{-1}$) following quenching collisions with highly vibrationally excited molecules.[4,5] These events correspond to the strongest collisions (i.e., large-$\Delta E$ collisions) but make up only a small fraction of energy transfer events. Weak collisions that transfer small amounts of energy are far more likely to occur, but their characterization poses a number of experimental challenges. Recent advances in transient IR absorption techniques have made it possible to extend previous studies into the realm of small-$\Delta E$ energy transfer. Data of this type yield information about the complete energy transfer distribution as well experimentally measured collision rates.

The effectiveness of collisions at removing energy from activated molecules is typically reported relative to a collision rate. The collision rate is of great importance in a number of fields including collisional energy transfer,[6−8] unimolecular reactions,[9−11] and nucleation theory.[12−15] Collision rates have been measured for a few systems,[7,16−23] but for neutral molecules they are typically estimated using a Lennard−Jones interaction potential.[24] This potential depends on the distance between the colliding molecules and uses the average parameters of $\varepsilon$ to describe attractive interactions and $\sigma$ to estimate the distance where repulsive interactions take over. Orientation-dependent interactions are not accounted for in the Lennard−Jones potential, nor are hydrogen-bonding interactions. Using IR absorption to measure the outcome of collisions that involve the full range of energy transfer values directly yields a measure of the collision rate. These data provide a benchmark for establishing how well the Lennard−Jones model describes collisions between molecules.

Recently, we have extended high resolution transient IR absorption probing into the low-$\Delta E$ regime to study the collisional quenching of pyrazine(E) with HOD.[25,26] This initial study characterized the full state-resolved energy transfer distribution and showed that the pyrazine/HOD collision rate is 1.7 times larger than the Lennard−Jones collision rate. Here we investigate how collision rates are affected by the presence of methyl groups on the donor molecule by measuring the collision dynamics of highly vibrationally excited 2-methylpyridine (2-picoline) and 2,6-dimethylpyridine (2,6-lutidine). Table 1 lists the physical properties of these molecules along with those for pyrazine. Ideally, results for the methylated donors would be compared to pyridine quenching data, but transient signals for pyridine collisions were too small. Instead the results are compared with pyrazine collisions.

Average energy transfer measurements show that polar molecules such as $H_2O$ and $NH_3$ are more efficient quenchers of highly excited molecules than nonpolar collision partners such as $CO_2$.[27−35] However, state-resolved energy gain data show that $H_2O$ is much less likely than $CO_2$ to be involved in large-$\Delta E$ quenching collisions with highly excited aromatic molecules.[5,36,37] Understanding the fundamental reasons for differences in average energy transfer behavior requires knowledge of the full energy transfer distribution as well as the collision rate.

Several other experimental methods have been used to study the energy transfer distribution function of highly excited molecules. Kinetically controlled selective ionization (KCSI) [38−41] has been developed and used by Luther and co-workers to directly monitor highly vibrationally excited donor molecules as they are relaxed by collisions. Distributions of highly

† Part of the "George C. Schatz Festschrift" special issue.

* To whom correspondence should be addressed.

10.1021/jp811077p CCC: $40.75 
Published on Web 03/20/2009

**TABLE 1: Summary of Physical Properties for Highly Vibrationally Excited Donor Molecules**

| donor molecule | pyrazine | 2-picoline | 2,6-lutidine |
|---|---|---|---|
| Lennard−Jones diameter $\sigma$ (Å) | 5.35[a] | 5.58[b] | 5.89[b] |
| Lennard−Jones well depth $\varepsilon$ (K) | 435.5 [a] | 465.8[c] | 467.9[c] |
| number of vibrational modes | 24 | 36 | 45 |
| mass (g/mol) | 80.09 | 93.13 | 107.16 |
| Lennard−Jones collision rate ($10^{-10}$ cm$^3$molecule$^{-1}$s$^{-1}$)[d] | 6.19 | 6.44 | 6.86 |

[a] Lennard−Jones parameters $\sigma$ and $\varepsilon$ for pyrazine are from the literature.[70] [b] Calculated using critical volume: $\sigma^3 \approx (9/8)(V_c/\pi N_A)$,[71] where $N_A$ is Avogadro's number. $V_c$ value for 2-picoline is $V_c$ = 292 cm$^3$ from the literature.[56] The $V_c$ value for 2,6-lutidine is estimated to be $V_c$ = 343 cm$^3$ determined by extrapolating from $V_c$ values for pyridine ($V_c$ = 243 cm$^3$)[56] and 2-picoline plotted as a function of $T_c$ (see footnote c). [c] Calculated using critical temperature: $\varepsilon \approx (3/4)T_c$.[71] $T_c$ values for 2-picoline and 2,6-lutidine are $T_c$ = 621 K and $T_c$ = 623.8 K, respectively, from the literature.[56] The value for pyridine is $T_c$ = 620 K. [d] The collision rate constants were determined using a Lennard−Jones potential as the intermolecular potential during the donor/HOD collisions.[19] The collision rate constants for donor/bath were determined using a Lennard−Jones (LJ) potential[19] given by $k_{LJ} = ((8k_BT)/\pi\mu)^{1/2} \Omega^{(2,2)*}\pi\sigma^2$, where the collision integral $\Omega^{(2,2)*}$ is a function of the reduced temperature $T^*$. $\Omega^{(2,2)*} = 1.16145(T^*)^{-0.14874} + 0.52487 \exp\{-0.7732T^*\} + 2.16178 \exp\{-2.43787T^*\}$, where $T^* = k_BT/\varepsilon$. The Lennard−Jones parameters $\sigma$ and $\varepsilon/k_B$ for the mixed donor/bath systems are obtained using established combining rules:[19] $\sigma = (\sigma_{donor} + \sigma_{bath})/2$ and $(\varepsilon/k_B) = ((\varepsilon/k_B)_{donor}(\varepsilon/k_B)_{bath})^{1/2}$. Values of $\sigma_{HOD}$ and $(\varepsilon/k_B)_{HOD}$ are the same as those for $H_2O$. Only mass differences are considered in the calculation. For $H_2O$, $\sigma_{H_2O}$ = 2.65 Å, $(\varepsilon/k_B)_{H_2O}$ = 380.0 K.[24]

vibrationally excited molecules with initial energy E are monitored as they pass through experimentally determined energy windows at an energy E′.[42−45] The molecular beam imaging technique of Ni and co-workers measures the velocity mapping of scattered molecules to measure the energy transfer distribution function.[46−48]

In this paper, we report the energy transfer dynamics for collisions of 2-picoline(E) and 2,6-lutidine(E) with HOD. High resolution transient IR absorption is used to measure the state-resolved appearance and product state distributions of scattered HOD molecules in rotational states with $E_{rot}$ = 109 to 1331 cm$^{-1}$. These measurements provide a complete description of the rotational and translational energy distributions of the HOD(000) products as well as a measure of the collision rate. The results are compared with those for pyrazine(E)/HOD collisions,[25,26] and the influence of donor methylation on collision rates and energy transfer profiles is discussed.

## Experimental Methods

A high-resolution transient IR laser absorption spectrometer was used to measure state-resolved energy gain profiles in HOD molecules that scatter from highly vibrationally excited 2-picoline ($E$ = 38 310 cm$^{-1}$) and 2,6-lutidine ($E$ = 38 700 cm$^{-1}$). The highly excited donors were prepared by radiationless decay to the ground electronic state following pulsed UV excitation using $\lambda$ = 266 nm light from the fourth harmonic of Nd:YAG laser.[49] The pulsed UV light excited the donor molecules at a repetition rate of 2 Hz. The UV power was kept below 4.2 MW/cm$^2$ to maximize signal-to-noise ratios while maintaining single-photon absorption of donor molecules.

A tunable single-mode F-center laser operating near $\lambda$ = 2.7 $\mu$m was used to measure transient IR absorption for individual rotational states of HOD using (001←000) transitions following collisions with excited donor molecules. The IR laser has a resolution of $\Delta\nu_{IR}$ = 0.0003 cm$^{-1}$ that is high enough to measure Doppler broadened line profiles for individual rotational states of HOD. Transient line profiles were measured by collecting transient IR absorption as a function of IR wavelength. The F-center laser was locked to a single cavity mode while an intracavity etalon tuned synchronously with a pair of rotating calcium fluoride plates. Typically a single cavity mode could be tuned over a wavelength range of 0.07 cm$^{-1}$.

The IR probe passed through a 3 m collision cell collinearly with the 266 nm pump light. The cell contained a flowing mixture of 2-picoline or 2,6-lutidine and the $H_2O$/HOD/$D_2O$ bath at a total pressure of ∼25 mTorr. With these conditions, about 15% of donor molecules were vibrationally excited and the average collision time is $\tau_{col} \sim 3$ $\mu$s, based on Lennard−Jones interactions. Linear transient absorption signals from $t$ = 0 to 1 $\mu$s correspond to nascent population changes of scattered HOD molecules determined using the method of initial rates. Deviations from linear absorption due to secondary quenching collisions were observed at times longer than 2 $\mu$s.

The HOD sample was prepared by mixing equal volumes of $H_2O$ and $D_2O$. At equilibrium, the $H_2O$/HOD/$D_2O$ sample had 49.4% HOD.[50] The pressure of donor and $H_2O$/HOD/$D_2O$ mixture was 1:2 in the collision cell in order to match a 1:1 ratio for donor and HOD. HPLC grade $H_2O$ and $D_2O$ (Cambridge Isotope Laboratories, 99.9%) was purified by several freeze/pump/thaw cycles to prevent the presence of atmospheric gases. 2-Picoline (Aldrich, 99+ %) and 2,6-lutidine (Aldrich, 99+ %) were purified by several freeze/pump/thaw cycles before use.

## Results and Discussion

**Transient Absorption of Scattered HOD(000) Molecules.** HOD molecules at room temperature change their translational and rotational energies after collisions with vibrationally hot donor molecules as shown in eq 1.

$$\text{donor}(E) + \text{HOD}(298\ \text{K}) \rightarrow \text{donor}(E') + \text{HOD}(000, J_{K_aK_c}, V) \quad (1)$$

Here $E$ = 38 310 cm$^{-1}$ for 2-picoline and 38 700 cm$^{-1}$ for 2,6-lutidine. $J$ is the total angular momentum of HOD, and $K_a$ and $K_c$ are the components along the molecular A axis and C axis, respectively. $V$ is the component of the velocity along the IR beam corresponding to a 1-D projection of a 3-D velocity vector spread.

High-resolution IR absorption of transitions involving HOD(000, $J_{K_a,K_c}$, $V$) monitors time-dependent population changes for individual $J$ states due to collisions with the hot donor molecules, as shown in eq 2.

$$\text{HOD}(000, J_{K_aK_c}, V) + \text{IR} \rightarrow \text{HOD}(001, J'_{Ka',Kc'}\ V) \quad (2)$$

Transient signals at $t$ = 1 $\mu$s were used to determine nascent population changes from collisions between highly vibrationally excited donor molecules and HOD.

The use of high-resolution IR transient absorption to measure strong collisions has been reported previously.[5] Probing the outcome of strong collisions involves monitoring bath molecules that are scattered into high rotational states that have essentially no population at 298 K. In this case, transient absorption signals correspond purely to the appearance of population in the state being probed. Measurements on weak collisions involving low-$J$

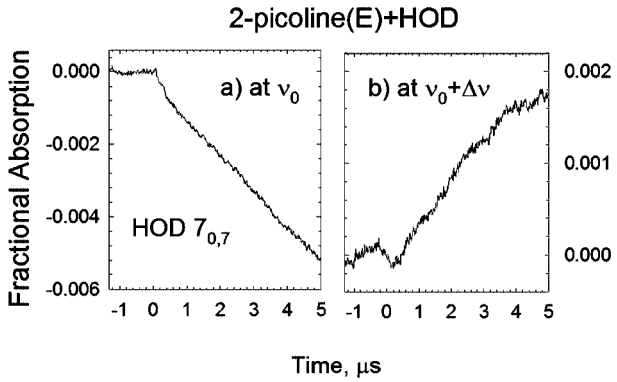


**Figure 1.** Fractional IR absorption of HOD(000) following collisions of highly excited 2-picoline with HOD as a function of time following UV excitation. Figure 1a shows depletion of HOD(000, $7_{0,7}$) with $E_{rot} = 403$ cm$^{-1}$ measured at $\nu_0$, and Figure 1b shows appearance for the same transition measured at $\Delta\nu = 0.01$ cm$^{-1}$ from line center.

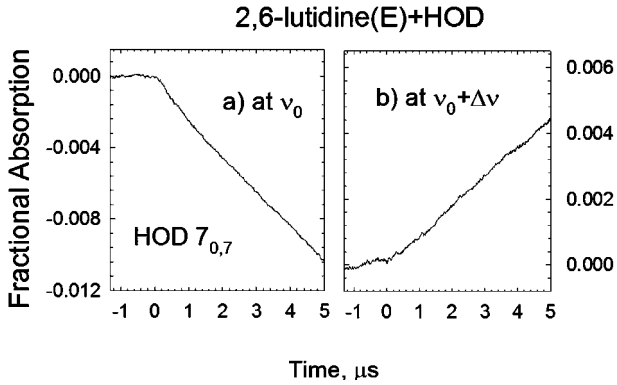


**Figure 2.** Fractional IR absorption of HOD(000) following collisions of highly excited 2,6-lutidine with HOD as a function of time following UV excitation. Figure 2a shows depletion of HOD(000, $7_{0,7}$) with $E_{rot} = 403$ cm$^{-1}$ measured at $\nu_0$ and Figure 2b shows appearance for the same transition measured at $\Delta\nu = 0.01$ cm$^{-1}$ from line center.

states of bath molecules have added complications. Substantial thermal population for low-$J$ states means that their transient signals are dominated by depletion which can overwhelm small appearance signals. If the Doppler-broadened line widths for appearance and depletion are equal, it is not possible to distinguish the relative transient populations. In addition, competing energy transfer pathways can interfere with pathway-specific absorption measurements by moving population into the upper state of the probe transition, since absorption gives information about the population *difference* between the two states of the transition. Collisions that put energy into the upper state of the probe transition will obscure measurements of the lower state population.

We consider the transient absorption of the HOD(000, $2_{2,0}$) state to illustrate our approach to probing weak collisions. The IR probe transition is HOD(001, $2_{2,1}$) ← HOD(000, $2_{2,0}$). The collision-induced population change for the (000, $2_{2,0}$) state results from two processes: HOD is scattered into the (000, $2_{2,0}$) state by eq 3 and depleted from this state by eq 4.

$$\text{donor}(E) + \text{HOD(any state)} \xrightarrow{k^J_{app}} \text{donor}(E') + \text{HOD}(000, 2_{2,0}) \quad (3)$$

$$\text{donor}(E) + \text{HOD}(000, 2_{2,0}) \xrightarrow{k^J_{dep}} \text{donor}(E') + \text{HOD(any state)} \quad (4)$$

Collisions can also directly populate the upper state of the probe transition, as shown in eq 5.

$$\text{donor}(E) + \text{HOD(298 K)} \rightarrow \text{donor}(E') + \text{HOD}(001, 2_{2,1}) \quad (5)$$

The collision-induced appearance for a number of HOD(001, $J_{K_a,K_c}$) states was investigated separately using HOD(002←001) probe transitions, but no transient absorption signals were observed. It is not surprising that collisions leading to energy gain in the (001) state are not observed. It is likely that vibration-to-vibration (V→V) energy transfer is dominated by a one-quantum transfer. The highest frequency vibrational modes of 2-picoline and 2,6-lutidine are near 3000 cm$^{-1}$ while the HOD $\nu_3$ stretch is near 3710 cm$^{-1}$. Thus, eq 5 does not impact the HOD(001←000) probe transitions in this study, and transient signals result purely from collisions described by eqs 3 and 4. For this reason, HOD(001←000) transitions can be used to characterize the energy partitioning in weak collisions of highly vibrationally excited donor molecules with HOD.

Transient fractional absorption was measured for a number of HOD(000) rotational states. Transient signals for the (000, $7_{0,7}$) state following collisions with highly vibrationally excited 2-picoline and 2,6-lutidine molecules are shown in Figures 1 and 2. The $7_{0,7}$ state has an energy of $E_{rot} = 403$ cm$^{-1}$ and is well populated at 298 K. At $\nu_0$, the center of the IR transition, the rate of population loss for this state is greater than appearance and negative-going signals are observed corresponding to net depletion of population. These are shown in Figures 1a and 2a. When the IR probe is tuned to the wings of the absorption as in Figures 1b and 2b, the transient absorption traces are positive-going, showing appearance of population in this state. Analysis of the transient line profiles yield quantitative information about the appearance and depletion populations, as described in the next section.

**Translational Energy of Collision Products.** The translational energy gain of scattered HOD(000) was measured for weak and strong collisions with both donor molecules using Doppler-broadened line profiles. The outcome of weak collisions was measured from the early time appearance of HOD molecules in low-$J$ states with $E_{rot} < 500$ cm$^{-1}$. These states have substantial ambient population at 298 K, and their transient profiles show both appearance and depletion behavior.

Figure 3 shows the transient line profile for the HOD $7_{0,7}$ state following collisions with 2,6-lutidine ($E$) based on transient signals at $t = 1$ $\mu$s. The signals at line center show negative-going depletion of the initial thermal population. A second positive-going component is seen in the wings of the line profile at approximately $\Delta\nu = 0.0125$ cm$^{-1}$ from line center. The positive-going component corresponds to appearance of molecules in the $7_{0,7}$ state and is a measure of the population and velocity distribution for a subset of weak collisions.

Doppler-broadened line profiles are fit using a nonlinear least-squares analysis to a double Gaussian function:[26]

$$F(\nu) = I_{app}\exp\left(-4\ln 2\left(\frac{\nu-\nu_0}{\Delta\nu_{app}}\right)^2\right) - I_{dep}\exp\left(-4\ln 2\left(\frac{\nu-\nu_0}{\Delta\nu_{dep}}\right)^2\right) + F_0 \quad (6)$$

The parameters $I_{app}$ and $I_{dep}$ are the appearance and depletion intensities at the center frequency $\nu_0$, and $\Delta\nu_{app}$ and $\Delta\nu_{dep}$ are the full width at half-maximum (fwhm) line widths for the absorption and depletion, respectively. $F_0$ accounts for small intensity shifts in baseline absorption. Values of $\Delta\nu_{app}$ were used to determine the translational temperatures of the scattered molecules in the laboratory frame ($T_{trans,lab}$) and the center of mass frame ($T_{rel}$).

The outcome of strong collisions was measured from the early time appearance of HOD molecules in high-$J$ states with $E_{rot} > 1000$ cm$^{-1}$. These states have negligible ambient population at 298 K and appearance signals are solely seen. The nascent line profiles for these states are fit to a single Gaussian function using eq 6 with $I_{dep} = 0$.

The appearance line widths and translational temperatures for a number of HOD(000) states due to collisions with hot donor molecules are listed in Table 2 and plotted in Figure 4, along with previous results for pyrazine/HOD collisions.[26] The product translational energy distributions are similar for collisions of pyrazine, picoline and lutidine and have temperatures of $T_{rel} \sim 500-800$ K. The product translational energies increase slightly as a function of HOD rotational energy, although the differences are within experimental error. Line profiles for the high-$J$ states (in gray) were measured prior to the low-$J$ states (in black) using a different experimental configuration and differences in etalon calibration may affect the line widths. Each line width listed in Table 2 is an average of three measurements, and the reported uncertainty is based on multiple measurements of room temperature line widths of a $CO_2$ ($10^01 \rightarrow 00^00$) transition that agreed with the known value to within 0.0005 cm$^{-1}$.

Relatively small amounts of translational energy are observed in the scattered molecules relative to the internal energy of the highly excited donor molecules, at least for the HOD states we have measured. The average appearance line widths for HOD(000) after single collisions with pyrazine, 2-picoline, and 2,6-lutidine/HOD are $\Delta\nu_{app} = 0.0148 \pm 0.001$, $0.0154 \pm 0.001$, and $0.0147 \pm 0.001$ cm$^{-1}$, respectively, corresponding to average laboratory frame translational temperatures of $T_{trans,lab} = 570 \pm 86$, $614 \pm 110$, and $575 \pm 109$ K. The corresponding center of mass frame temperatures are $T_{rel} = 635 \pm 95$ K, $678 \pm 123$ K, and $624 \pm 118$ K. The average changes in relative translational energy are $\langle\Delta E_{rel}\rangle = 351 \pm 49$, $397 \pm 71$, and $340 \pm 63$ cm$^{-1}$ for pyrazine, picoline, and lutidine collisions, based on $\langle\Delta E_{rel}\rangle = {}^3/_2 k_B(T_{rel} - T_0)$. It is interesting that the recoil energies are very close to ${}^3/_2 k_B T_0$ where $T_0 = 298$ K for the initial velocity distribution. The excited donor molecules contain more than 38 000 cm$^{-1}$ of vibrational energy yet collisions impart only ~1% of this energy into translational motion of the products. Of course, higher energy HOD states may be scattered with more translational energy, but based on the rotational distributions presented in the next section, the probability of such collisions is likely to be very small.

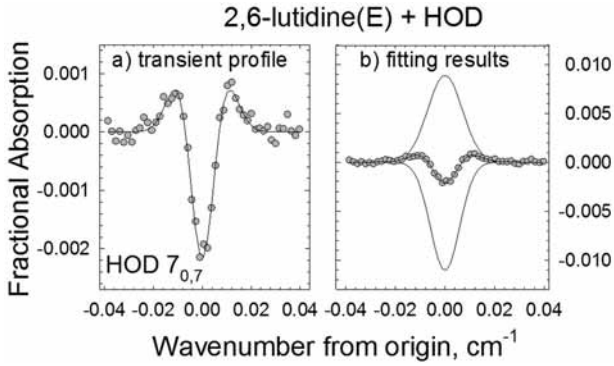


**Figure 3.** Transient absorption line profile for HOD(000, $7_{0,7}$) collected at 1 $\mu$s following UV excitation of 2,6-lutidine. The raw data and fit are shown in Figure 3a while the double Gaussian fit alone is shown in Figure 3b. The fit has been separated into its absorption (dashed line/positive going) and depletion (dashed line/negative going) components for clarity.

The depletion signals give information about the velocity distributions of the initial HOD molecules. The translational temperatures for depletion are listed in Table 3 and have values that are within error of $T = 298$ K. For 2-picoline/HOD collisions, the average laboratory frame depletion temperature is $T_{dep} = 368 \pm 81$ K. Similarly, 2,6-lutidine/HOD has $T_{dep} = 376 \pm 71$ K. For pyrazine/ HOD collisions, the depletion profiles have temperatures of $T_{dep} = 315-350$ K. The data may indicate that the precollision distribution of HOD molecules is shifted to slightly higher velocities than room temperature, but we note that the effect is fairly small, if it is there at all.

**Rotational Energy Gain of HOD(000).** Nascent rotational distributions of scattered HOD(000) molecules were measured for collisions with picoline($E$) and lutidine($E$). Early time population changes for a number of HOD rotational states with $E_{rot} = 109$ to 1330 cm$^{-1}$ were fit with a Boltzmann distribution for each donor. The data and the fits are shown in Figure 5, along with earlier data for collisions with pyrazine. The rotational energy distributions of HOD are similar for the three donors. For picoline/HOD collisions, the rotational temperature of scattered HOD is $T_{rot} = 426 \pm 60$ K. For lutidine/HOD collisions, $T_{rot} = 394 \pm 64$ K. For pyrazine/HOD collisions, $T_{rot} = 430 \pm 50$ K. The average change in HOD rotational energy is relatively small for each donor/HOD pair. Using $\langle\Delta E_{rot}\rangle = {}^3/_2 k_B(T_{rot} - T_0)$ and $T_0 = 298$ K, we find that $\langle\Delta E_{rot}\rangle = 133 \pm 63$, $100 \pm 67$, and $138 \pm 52$ cm$^{-1}$, respectively for collisions with picoline, lutidine, and pyrazine.

The HOD(000) molecules scattered from pyrazine($E$), picoline($E$), and lutidine($E$) have rotational distributions that are all near $T_{rot} = 400$ K, but other studies have shown that collisions with $H_2O$ are quite different. In strong collisions with the same highly excited donors (also prepared with 266 nm light), $H_2O$ is scattered into higher energy rotational states than HOD, and with broader rotational distributions that depend on the identity of the collision partner. In pyrazine/$H_2O$ collisions, $H_2O$ is scattered with a rotational temperature is $T_{rot} = 920 \pm 100$ K.[5] Collisions of $H_2O$ with picoline and lutidine impart less rotational energy to the $H_2O$ bath, with nascent rotational temperatures of $T_{rot} = 590 \pm 90$ K and $490 \pm 80$ K, respectively.[4,51]

It is likely that hydrogen bonding interactions are involved in HOD and $H_2O$ quenching collisions and that stronger hydrogen bonding interactions for HOD end up reducing its rotational energy gain through collisions. Water has two sites for hydrogen bonding with nitrogen-containing aromatics. The O−H bond of water interacts with the nitrogen lone pair through a $\sigma$-type interaction, and the $\pi$-cloud of the aromatic interacts with the two hydrogen atoms of water in a $\pi$-type interaction.[52,53] There is spectroscopic evidence from Zwier and co-workers that in water complexes with nitrogen-containing aromatics, $H_2O$ undergoes shuttling motion between local minima of the $\sigma$- and

**TABLE 2: Transient Line Widths and Translational Energy Gain Measurements for HOD(000, $J_{K_a,K_c}$) Rotational States Following Collisions with Highly Vibrationally Excited 2-Picoline ($E = 38\,310$ cm$^{-1}$) and 2,6-Lutidine ($E = 38\,700$ cm$^{-1}$)**

| donor | HOD $J_{K_a,K_c}$ | $\nu_0$ (cm$^{-1}$) | $E_{rot}$ (cm$^{-1}$) | $\Delta\nu_{app}$[a](cm$^{-1}$) | $T_{trans,lab}$[b] (K) | $T_{rel}$[c] (K) | $\Delta E_{rel}$[d] (cm$^{-1}$) |
|---|---|---|---|---|---|---|---|
| picoline | $2_{2,0}$ | 3702.904 | 109.269 | 0.0137 | 500 ± 75 | 541 ± 81 | 254 ± 38 |
| | $4_{1,3}$ | 3787.510 | 182.983 | 0.0161 | 670 ± 100 | 746 ± 111 | 467 ± 70 |
| | $6_{1,6}$ | 3798.189 | 308.615 | 0.0139 | 500 ± 90 | 541 ± 97 | 254 ± 46 |
| | $7_{0,7}$ | 3810.595 | 403.161 | 0.0163 | 685 ± 145 | 764 ± 162 | 486 ± 103 |
| | $7_{1,6}$ | 3826.241 | 473.918 | 0.0153 | 595 ± 140 | 656 ± 154 | 373 ± 88 |
| | $11_{1,10}$ | 3866.368 | 1046.474 | 0.0172 | 733 ± 110 | >822 ± 132 | 546 ± 82 |
| lutidine | $2_{2,0}$ | 3702.904 | 109.269 | 0.0138 | 514 ± 80 | 552 ± 86 | 265 ± 41 |
| | $4_{1,3}$ | 3787.510 | 182.983 | 0.0136 | 477 ± 105 | 509 ± 112 | 220 ± 48 |
| | $6_{1,6}$ | 3798.189 | 308.615 | 0.0138 | 610 ± 125 | 665 ± 136 | 383 ± 78 |
| | $7_{0,7}$ | 3810.595 | 403.161 | 0.0133 | 559 ± 140 | 605 ± 152 | 320 ± 80 |
| | $7_{1,6}$ | 3826.241 | 473.918 | 0.0149 | 484 ± 105 | 517 ± 112 | 228 ± 50 |
| | $11_{1,10}$ | 3866.368 | 1046.474 | 0.0165 | 677 ± 100 | 744 ± 112 | 465 ± 70 |
| | $12_{1,11}$ | 3876.128 | 1220.027 | 0.0169 | 707 ± 106 | 780 ± 117 | 502 ± 75 |

[a] $\Delta\nu_{app}$ is the full width at half-maximum (FHWM) line width for a specific $J_{K_a,K_c}$ state of HOD measured at 1 $\mu$s following the UV pulse. Each value is an average of typically three values and has an uncertainty of 0.0007 cm$^{-1}$. [b] Laboratory frame translational temperature for HOD(000, $J_{K_a,K_c}$) is determined using $T_{trans,lab} = (mc^2/8R\ \ln(2))(\Delta\nu_{app}/\nu_o)^2$. The uncertainty is determined from both measurement uncertainty in the line width and propagated error in the double Gaussian fit. [c] Center-of-mass frame translational temperature for HOD(000, $J_{K_a,K_c}$) is determined using $T_{rel} = T_{trans,lab} + (T_{trans,lab} - 298)(m_{HOD}/m_{donor})$ [d] Average translational energy change for HOD(000, $J_{K_a,K_c}$) is obtained using $\langle\Delta E_{rel}\rangle = {}^3/_2 k_B(T_{rel} - T_0)$, where $T_0 = 298$ K.

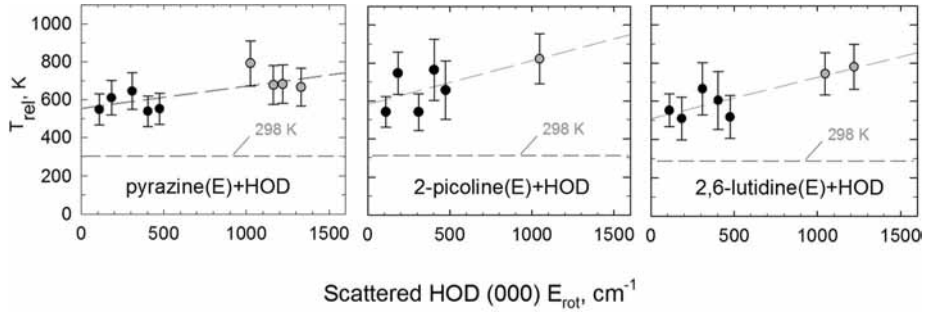


**Figure 4.** Center-of-mass translational temperatures ($T_{rel}$) vs HOD(000) $E_{rot}$ following collisions with pyrazine, 2-picoline, and 2,6-lutidine. $T_{rel}$ does not have a strong dependence on $E_{rot}$ from 0 cm$^{-1}$ to 1500 cm$^{-1}$.

**TABLE 3: Transient Line Widths and Translational Energy Profiles for Population Depletion of HOD(000, $J_{K_a,K_c}$) Rotational States Due to Collisions with Highly Vibrationally Excited 2-Picoline ($E = 38\,310$ cm$^{-1}$) and 2,6-Lutidine ($E = 38\,700$ cm$^{-1}$)**

| donor molecule | $J_{K_a,K_c}$ | $\Delta\nu_{dep}$ (cm$^{-1}$)[a] | $T_{dep}$[b] (K) |
|---|---|---|---|
| 2-picoline | $2_{2,0}$ | 0.0114 | 353 ± 43 |
| | $4_{1,3}$ | 0.0125 | 405 ± 45 |
| | $6_{1,6}$ | 0.0108 | 301 ± 39 |
| | $7_{0,7}$ | 0.0125 | 401 ± 45 |
| | $7_{1,6}$ | 0.0122 | 379 ± 43 |
| 2,6-lutidine | $2_{2,0}$ | 0.0118 | 374 ± 44 |
| | $4_{1,3}$ | 0.0119 | 368 ± 43 |
| | $6_{1,6}$ | 0.0126 | 433 ± 48 |
| | $7_{0,7}$ | 0.0122 | 382 ± 44 |
| | $7_{1,6}$ | 0.0113 | 322 ± 40 |

[a] $\Delta_{dep}$ is fwhm Doppler-broadened line width for population depletion from HOD states with $E_{rot} = 100-500$ cm$^{-1}$. [b] Laboratory-frame translational temperatures $T_{dep}$ for depletion of initial HOD(000, $J_{K_a,K_c}$) are determined similarly to $T_{trans,lab}$ in footnote b in Table 2 using $\Delta\nu_{dep}$.

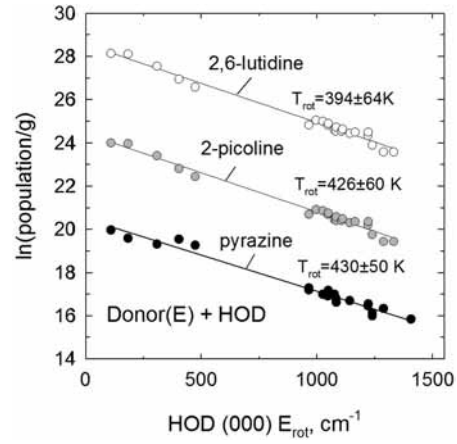


**Figure 5.** The nascent distributions of HOD(000) rotational states for collisions with highly vibrationally excited pyrazine (black circles), 2-picoline (gray circles), and 2,6-lutidine (open circles).

$\pi$-sites.[54] This type of directed motion between $\sigma$- and $\pi$-sites has also been implicated in the extent to which scattered water molecules contain excess rotational energy following collisions with substituted pyridines.[55] In methylpyridines, methyl groups adjacent to the nitrogen lone pair tend to enhance the strength of the $\sigma$-type hydrogen bond by donating electron density. This is supported by the increasing basicity of methylated pyridines.[56] Increasing the depth of one local minimum will tend to diminish directed movement to another minimum, thus reducing the extent of rotational energy gain in the scattered water molecules. This idea is consistent with our observation for the three donors considered here, namely that $H_2O$ is scattered from pyrazine($E$) with the largest amount of rotational energy while picoline and lutidine impart substantially less rotational energy to $H_2O$.

Differences in the intermolecular potentials of HOD and $H_2O$ with pyrazine provide insight into differences in the collision dynamics for these bath molecules. Caminati and co-workers measured the microwave spectra of pyrazine-water complexes in a molecular beam and only observed $\sigma$-type hydrogen

bonds.[52] This finding is consistent with ab initio calculations showing that $\sigma$-type hydrogen bond in pyrazine−$H_2O$ has an interaction energy of ∼5 kcal/mol and that the $\pi$-hydrogen bond for benzene−$H_2O$ is ∼2 kcal/mol. Furthermore, Caminati and co-workers concluded that the pyrazine:HOD bond is stronger than the pyrazine:$H_2O$ bond based on the observation that the pyrazine−HOD complex is observed in the molecular beam exclusively with the D-atom of HOD bonded to the nitrogen lone pair. Johnson and co-workers have shown that the most stable configuration for complexes of atomic ions with $H_2O$, HOD, and $D_2O$ results from a balance of hydrogen bond strength and shifts in vibrational frequencies and zero-point energies that depend on hydrogen bond strength.[57] If the local minimum of the $\sigma$-type hydrogen bond for pyrazine/HOD is deep enough, it will suppress directed motion between $\sigma$- and $\pi$-sites that leads to enhancements in rotation of the scattered HOD molecules.[25,26] Of course, this does not imply that collisions with HOD only involve geometries associated with the $\sigma$-type local minima since numerous molecular orientations are possible for collisions, and it is unlikely that complexes are formed at 300 K. Rather, the presence of multiple local minima that are accessible in collisions with $H_2O$ can lead to motion that enhances water's rotational energy. In cases where this directed motion is reduced, water's rotational energy will also be diminished.

Other factors could be important as well. Differences in the energy content of the hot donor may affect the extent of rotational energy in the scattered molecules. The donor vibrational temperature $T_{vib}$ is defined as the vibrational distribution for which the mean vibrational energy is the same as the internal energy $E$ of the hot donor. In our experiments, $T_{vib} = 4020$ K for pyrazine($E$), 2440 K for 2-picoline($E$), and 1990 K for 2,6-lutidine($E$). We observe nascent $T_{rot}$ values for $H_2O$ that are proportional to the donor $T_{vib}$ values. If this is an important factor, then it is not clear why $H_2O$ collisions would be sensitive to the donor energy content while HOD collisions are not.

Another factor to consider is the rotational state structure of $H_2O$ and HOD. HOD has a higher rotational state density than $H_2O$ due to differences in moments of inertia and degeneracy factors. The A, B, and C rotational constants for HOD are roughly one-third smaller than those for $H_2O$ leading to more closely spaced rotational states in HOD. In addition, HOD has a nuclear spin degeneracy of $g_{ns} = 6$ for all rotational states while for $H_2O$, $g_{ns} = 3$ for states with odd ($K_a + K_c$) and $g_{ns} = 1$ for states with even ($K_a + K_c$). The upshot is that there are more HOD states than $H_2O$ states with $E_{rot} < 1000$ cm$^{-1}$ by a factor of 4. Small angular momentum changes are favored in collisions, which in turn favor a narrower distribution of final states for HOD. Details of the exact ordering of angular momentum states for $H_2O$ and HOD could lead to the observed differences in the rotational distributions. Studies on $D_2O$ collisions would help address these issues.

**Energy Transfer Rates from HOD(000) Appearance Measurements.** State-specific bimolecular energy transfer rate constants $k_{app}^J$ (in eq 3) for collisions of 2-picoline($E$) and 2,6-lutidine($E$) with HOD were determined by transient absorption measurements for a number of HOD rotational states that are listed in Tables 4 and 5. The states listed in Tables 4 and 5 are a subset of all HOD rotational states. Rate constant for states not listed in Tables 4 and 5 were determined using the experimentally measured HOD rotational temperatures (Figure 5). The sets of total rate constants are shown in Figure 6 along with rates for pyrazine−HOD collisions. The rates shown in Figure 6 are for the complete HOD(000) distribution that comes from vibration-to-rotation/translation (V−RT) energy transfer.

**TABLE 4: Observed Appearance Rates of HOD(000, $J_{K_a,K_c}$) Due to Collisions with 2-Picoline ($E = 38\,310$ cm$^{-1}$)**

$$\text{donor}(E) + \text{HOD} \xrightarrow{k_{app}^J} \text{donor}(E - \Delta E) + \text{HOD}(000, J_{K_aK_c})$$

| $J_{K_a,K_c}$ | $\nu_0$, cm$^{-1}$ | $E_{rot}$, cm$^{-1}$ | $k_{app}^J$, $10^{-12}$ cm$^3$ molecule$^{-1}$ s$^{-1}$ |
|---|---|---|---|
| $2_{2,0}$ | 3702.904 | 109.269 | 20.9 ± 6.3 |
| $4_{1,3}$ | 3787.510 | 182.984 | 29.7 ± 8.9 |
| $6_{1,6}$ | 3798.189 | 308.616 | 28.5 ± 8.6 |
| $7_{0,7}$ | 3810.595 | 403.162 | 24.2 ± 7.3 |
| $7_{1,6}$ | 3826.241 | 473.918 | 19.2 ± 5.8 |
| $10_{2,8}$ | 3757.296 | 964.851 | 5.5 ± 1.7 |
| $10_{3,8}$ | 3860.956 | 995.793 | 5.0 ± 1.5 |
| $10_{3,7}$ | 3879.275 | 1024.569 | 4.5 ± 1.4 |
| $11_{1,10}$ | 3866.368 | 1046.474 | 4.6 ± 1.4 |
| $11_{2,10}$ | 3864.729 | 1049.125 | 4.6 ± 1.4 |
| $12_{1,12}$ | 3864.216 | 1075.763 | 4.6 ± 1.4 |
| $9_{5,5}$ | 3835.743 | 1082.785 | 3.4 ± 1.0 |
| $9_{5,4}$ | 3836.070 | 1082.887 | 3.4 ± 1.0 |
| $10_{4,7}$ | 3859.538 | 1106.264 | 3.5 ± 1.1 |
| $10_{4,6}$ | 3866.258 | 1110.760 | 3.4 ± 1.0 |
| $11_{2,9}$ | 3884.079 | 1141.692 | 3.4 ± 1.0 |
| $11_{3,9}$ | 3873.111 | 1164.509 | 3.1 ± 0.9 |
| $12_{1,11}$ | 3876.128 | 1220.029 | 2.9 ± 0.9 |
| $12_{2,11}$ | 3875.159 | 1221.537 | 2.8 ± 0.8 |
| $10_{5,6}$ | 3850.937 | 1238.795 | 2.2 ± 0.7 |
| $11_{4,7}$ | 3884.345 | 1287.239 | 2.1 ± 0.6 |
| $12_{2,10}$ | 3893.025 | 1331.216 | 2.0 ± 0.6 |
| $k_{app} = \sum_J k_{app}^J = (1.6 \pm 0.5) \times 10^{-9}$ cm$^3$ molecule$^{-1}$ s$^{-1}$ [a] | | | |

[a] A subset of HOD product states have been measured to determine appearance rates. The total appearance rate constant $k_{app}$ is a sum of rate constants for al HOD states, based on the rates listed above and the nascent HOD rotational temperature (Figure 5) resulting from collisions with excited picoline.

Since the HOD rotational distributions are nearly the same, the distributions of $k_{app}^J$ are similar for the three donors. However, there are differences in the magnitude of the energy transfer rate constants. The integrated energy transfer rate constant $k_{app}$ for each donor is the sum of $k_{app}^J$ over all HOD(000) rotational states. The integrated rate constants are $k_{app} = (1.6 \pm 0.5) \times 10^{-9}$ cm$^3$ molecule$^{-1}$ s$^{-1}$ for 2-picoline/HOD and $k_{app} = (2.2 \pm 0.7) \times 10^{-9}$ cm$^3$ molecule$^{-1}$ s$^{-1}$ for 2,6-lutidine/HOD. For pyrazine/HOD, $k_{app} = (1.0 \pm 0.3) \times 10^{-9}$ cm$^3$ molecule$^{-1}$ s$^{-1}$.[25,26]

The V−RT relaxation pathway is the primary channel of collisional quenching for aromatic molecules with HOD. Energy transfer from donor vibration to bath vibration (V−V) is less likely for these collision partners, with typical rates that are a few percent or less of the collision rate. Transient signals for HOD(010) from 2-picoline and 2,6-lutidine collisions are below the detection limit of our experiments. In the case of pyrazine/$H_2O$, collisions that produce $H_2O$ (010) account for ∼5% of the total collision rate.[36] Also, no reactive pathways that produce HOD have been detected from collisions of vibrationally hot donors and $D_2O$. The integrated energy transfer rate based on the V−RT channel is a lower limit to the collision rate for each donor−acceptor pair.

**Collision Rates from Transient HOD Measurements.** State-resolved population depletion measurements are another measure of the collision rate and provide a consistency check with the total appearance rates. Collisions between highly vibrationally excited donor molecules and HOD move population out of low-$J$ HOD states that are populated at room temperature and into the final distribution of states. The rate

**TABLE 5: Observed Appearance Rates of HOD(000, $J_{K_a,K_c}$) Due to Collisions with 2,6-Lutidine ($E$ = 38 700 cm$^{-1}$)**

$$\text{donor}(E) + \text{HOD} \xrightarrow{k^J_{app}} \text{donor}(E - \Delta E) + \text{HOD}(000, J_{K_aK_c})$$

| $J_{K_a,K_c}$ | $\nu_0$, cm$^{-1}$ | $E_{rot}$, cm$^{-1}$ | $k^J_{app}$, $10^{-12}$ cm$^3$ molecule$^{-1}$ s$^{-1}$ |
|---|---|---|---|
| $2_{2,0}$ | 3702.904 | 109.269 | 32.9 ± 9.9 |
| $4_{1,3}$ | 3787.510 | 182.984 | 45.3 ± 13.6 |
| $6_{1,6}$ | 3798.189 | 308.616 | 41.5 ± 12.5 |
| $7_{0,7}$ | 3810.595 | 403.162 | 34.0 ± 10.2 |
| $7_{1,6}$ | 3826.241 | 473.918 | 26.3 ± 7.9 |
| $10_{2,8}$ | 3757.296 | 964.851 | 6.2 ± 1.9 |
| $10_{3,8}$ | 3860.956 | 995.793 | 5.6 ± 1.7 |
| $10_{3,7}$ | 3879.275 | 1024.569 | 5.0 ± 1.5 |
| $11_{1,10}$ | 3866.368 | 1046.474 | 5.1 ± 1.5 |
| $11_{2,10}$ | 3864.729 | 1049.125 | 5.0 ± 1.5 |
| $12_{1,12}$ | 3864.216 | 1075.763 | 5.0 ± 1.5 |
| $9_{5,5}$ | 3835.743 | 1082.785 | 3.7 ± 1.1 |
| $9_{5,4}$ | 3836.070 | 1082.887 | 3.7 ± 1.1 |
| $10_{4,7}$ | 3859.538 | 1106.264 | 3.7 ± 1.1 |
| $10_{4,6}$ | 3866.258 | 1110.760 | 3.7 ± 1.1 |
| $11_{2,9}$ | 3884.079 | 1141.692 | 3.6 ± 1.1 |
| $11_{3,9}$ | 3873.111 | 1164.509 | 3.3 ± 1.0 |
| $12_{1,11}$ | 3876.128 | 1220.029 | 3.0 ± 0.9 |
| $12_{2,11}$ | 3875.159 | 1221.537 | 2.9 ± 0.9 |
| $10_{5,6}$ | 3850.937 | 1238.795 | 2.3 ± 0.7 |
| $11_{4,7}$ | 3884.345 | 1287.239 | 2.1 ± 0.6 |
| $12_{2,10}$ | 3893.025 | 1331.216 | 2.0 ± 0.6 |

$k_{app} = \sum_J k^J_{app} = (2.2 \pm 0.7) \times 10^{-9}$ cm$^3$ molecule$^{-1}$ s$^{-1}$ [a]

[a] A subset of HOD product states have been measured to determine appearance rates. The total appearance rate constant $k_{app}$ is a sum of rate constants for al HOD states, based on the rates listed above and the nascent HOD rotational temperature (Figure 5) resulting from collisions with excited lutidine.

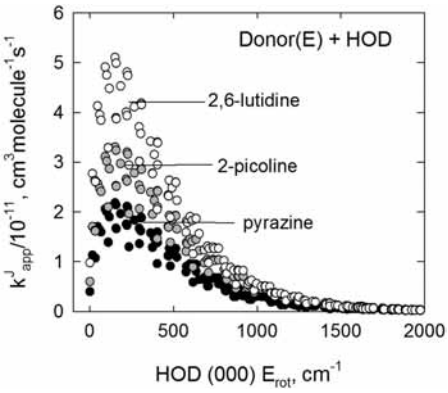


**Figure 6.** Rate constants $k^J_{app}$ for appearance of HOD(000) following collisions with highly vibrationally excited pyrazine, 2-picoline, and 2,6-lutidine. Values of $k^J_{app}$ for HOD include a nuclear spin degeneracy of $g_{ns} = 6$ and a rotational degeneracy of $g_{rot} = 2J + 1$ and are based on the rate constants in Table 6.

for depletion is given in eq 7, based on the idea that elastic and inelastic collisions change the velocity and/or rotational quantum state of HOD.

$$\text{rate}_{dep}(J) = -\frac{\text{d}[\text{HOD}^J]}{\text{d}t} = k_{dep}[\text{HOD}^J]_0[\text{donor}^E]_0 \quad (7)$$

Here $[\text{HOD}^J]_0$ is the initial concentration of HOD in a single rotational state. $[\text{donor}^E]_0$ is the initial concentration of highly vibrationally excited donor molecules determined from UV absorption measurements. Depletion of HOD population results solely from collisions in these measurements, so the depletion rate is essentially the collision rate. We assume to first order that the collision rate constant does not depend on $J$. The depletion rate constant $k_{dep}$ was measured for a number of HOD states based on the depletion component of individual line profiles (as in Figure 3), and values are listed in Table 6. The average depletion rate constants for pyrazine, 2- picoline/HOD, and 2,6-lutidine/HOD are $\langle k_{dep} \rangle = (1.1 \pm 0.3) \times 10^{-9}$, $(2.3 \pm 0.7) \times 10^{-9}$, and $(2.3 \pm 0.7) \times 10^{-9}$ cm$^3$ molecule$^{-1}$ s$^{-1}$. These are in reasonable agreement with the integrated appearance rates of $k_{app} = (1.0 \pm 0.3) \times 10^{-9}$ cm$^3$ molecule$^{-1}$ s$^{-1}$ for pyrazine/HOD, $k_{app} = (1.6 \pm 0.5) \times 10^{-9}$ cm$^3$ molecule$^{-1}$ s$^{-1}$ for 2-picoline/HOD and $k_{app} = (2.2 \pm 0.7) \times 10^{-9}$ cm$^3$ molecule$^{-1}$ s$^{-1}$ for 2,6-lutidine/HOD. We note that $k_{app} \leq k_{dep}$ for the three donor/HOD pairs considered here.

The appearance and depletion rates provide independent measures of the collision rate for donor/HOD collisions. The appearance rates account for the primary collision pathway of V−RT energy transfer and result from measurements of the full distribution of scattered molecules for this pathway. Appearance rates are a very good description of the collision rate since V−V energy transfer is about 100 times less likely than V−RT energy transfer. Depletion rates account for all energy transfer pathways and in theory are a better measure of the collision rate. However, the depletion rates are measured directly from a small number of individual HOD states and have larger uncertainty than the appearance rates. For this reason, the appearance rates $k_{app}$ are a better description of the experimentally measured collision rates.

**Comparison of Observed Collision Rates with Lennard−Jones Collision Rates.** Lennard−Jones collision rates are widely used as a reference in chemical kinetics. The Lennard−Jones potential is a two parameter ($\sigma$ and $\varepsilon$) description of molecular interactions that depends on the distance between molecules but does not account for orientational effects. The empirical parameters $\sigma$ (for size) and $\varepsilon$ (for attractive interactions) are determined from pure species and then combined to give average parameters to describe collisions of mixed species. The Lennard−Jones collision rates for the three donor-HOD pairs are listed in Table 1 and have values of $k_{LJ} \sim 6.5 \times 10^{-10}$ cm$^3$ molecule$^{-1}$ s$^{-1}$ at 298 K. The energy transfer rates for collisions of pyrazine, picoline, and lutidine with HOD are each larger than the Lennard−Jones collision rates. A comparison is shown in Figure 7. The experimentally determined collision rate is 1.7 times larger than the Lennard−Jones rate for pyrazine/HOD. The ratio of $k_{app}$ to $k_{LJ}$ for picoline/HOD collisions is 2.5 and for lutidine/HOD the ratio is 3.2. It is not surprising that the observed collision rates are larger than Lennard−Jones rates, based on the strong hydrogen bonding interactions of HOD with nitrogen-containing aromatics.

It is interesting that the observed enhancements in collision rates scale roughly with the basicity of the donor molecules. Pyrazine, picoline, and lutidine have p$K_b$ values of 13.4, 8.0, and 7.4, making lutidine the best electron donor of this group.[56,58] Dipole moments enhance collision rates through long-range attraction. The dipole moments of picoline ($\mu$ = 1.85 D)[56] and lutidine ($\mu$ = 1.65 D)[59] are comparable to one another while pyrazine has no dipole moment by symmetry. Long-range interactions may contribute to enhancements in the collision rate. If the enhancements are due solely to attractive interactions, then $\varepsilon$ values for the Lennard−Jones potential would have to increase by factors of ~3.7, ~48, and ~1040 for the pyrazine/HOD, 2-picoline/HOD, and 2,6-lutidine/HOD pairs. It is also

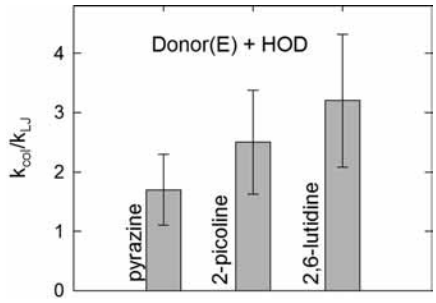


**Figure 7.** Bar graph showing the extent to which the collision rates determined experimentally in this work for collisions between highly vibrationally excited azabenzenes with HOD vary from the Lennard−Jones collision rate. The ratio of $k_{col}/k_{LJ}$ is a lower limit because of the possibility for pathways beyond HOD(000) scattering.

possible that large amplitude vibrational motion increases the effective size and polarizability of the vibrationally excited donors, thereby increasing the collision rate. Large amplitude motion due to ring breathing and torsion modes of the aromatic ring is likely to enhance the collision rate. Additional distortions are possible for the methyl groups of 2-picoline and 2,6-lutidine. The larger enhancements observed for the methylated donors is consistent with this idea. On the basis of the measured collision rates, the Lennard−Jones $\sigma$ parameter would have to increase by ∼1.4, ∼1.8, and ∼2.1 for pyrazine, 2-picoline, and 2,6-lutidine to account for deviations of $k_{app}$ from $k_{LJ}$. The effect of hydrogen bonding on the ratio of $k_{app}$ to $k_{LJ}$ can be tested by measuring $k_{app}$ for donor/bath pairs with a larger range of intermolecular interactions and basicity. Energy-dependent collision studies will elucidate the extent to which vibrational excitation increases effective molecular size.

To measure nascent energy distributions from collisions, it is necessary to detect populations of scattered molecules before they undergo secondary collisions. We have measured population changes at 1 $\mu$s following donor excitation based on the Lennard−Jones collision time of $t_{col} = 3$ $\mu$s for our experimental conditions. The experimental rates for excited donors with HOD are up to 3 times larger than Lennard Jones collision rates. This enhancement increases the rate of secondary collisions of the scattered HOD molecules and impacts the window for single collision measurements. However, the concentration of excited donor molecules is relatively small and accounts for only about 6% of the total number density. A kinetic analysis using experimental collision rates for excited donor/HOD collisions and Lennard−Jones rates for donor/HOD and water/HOD collisions shows that the average time between collisions is 2.3 $\mu$s in our measurements. The transient data are consistent with single-collision conditions for times up to $t = 2$ $\mu$s with signals that are linear and transient line profiles that are not narrowed as a function of time. Curvature and line narrowing are observed at longer times. Under our experimental conditions, the influence of secondary quenching collisions on data collected at 1 $\mu$s should be minimal.

**Energy Transfer Probability Distributions.** In order to investigate the role of state density in collisions of HOD with highly vibrationally excited pyrazine, 2-picoline, and 2,6-lutidine, complete energy transfer probability distributions were determined. These collision systems are the first for which complete $P(\Delta E)$ functions have been presented from state-resolved experimental data for molecules of this type. A detailed description of determining $P(\Delta E)$ from state-resolved data has been explained previously.[26] The following parameters were used from the experimental measurements described previously: center-of-mass translational temperatures ($T_{rel}$ in Table 2), energy transfer rates for individual states ($k^J_{app}$ in Table 4 and 5), and the temperature of the nascent rotational distribution ($T_{rot}$ in Figure 5). Translational temperatures were found depend only slightly on $E_{rot}$, so the average translational temperature across all states was used. For each donor/HOD pair, state-resolved energy transfer probabilities $P_J(\Delta E)$ were obtained using eq 8 and an energy transfer probability curve $P(\Delta E)$ resulted from summing over all states, $P(\Delta E) = \sum P_J(\Delta E)$.[26,60]

**TABLE 6: Depletion Rates of HOD(000, $J_{K_a,K_c}$) Due to Collisions with Pyrazine ($E$ = 37,900 cm$^{-1}$), 2-Picoline ($E$ = 38 310 cm$^{-1}$), and 2,6-Lutidine ($E$ = 38 700 cm$^{-1}$)**

$$\text{donor}(E) + \text{HOD}(000, J_{K_aK_c}) \xrightarrow{k_{dep}} \text{donor}(E - \Delta E) + \text{HOD}$$

| donor | HOD $J_{K_a,K_c}$ | $\nu_0$, cm$^{-1}$ | $E_{rot}$, cm$^{-1}$ | $k_{dep}$, 10$^{-9}$ cm$^3$ molecule$^{-1}$ s$^{-1}$ |
|---|---|---|---|---|
| pyrazine[a] | $2_{2,0}$ | 3702.904 | 109.269 | 1.2 ± 0.4 |
| | $4_{1,3}$ | 3787.510 | 182.984 | 0.9 ± 0.3 |
| | $6_{1,6}$ | 3798.189 | 308.616 | 1.0 ± 0.3 |
| | $7_{0,7}$ | 3810.595 | 403.162 | 1.2 ± 0.4 |
| | $7_{1,6}$ | 3826.241 | 473.918 | 1.1 ± 0.3 |
| | $\langle k_{dep}\rangle = (1.1 \pm 0.3) \times 10^{-9}$ cm$^3$ molecule$^{-1}$ s$^{-1}$ [b] | | | |
| 2-picoline | $2_{2,0}$ | 3702.904 | 109.269 | 2.3 ± 0.7 |
| | $4_{1,3}$ | 3787.510 | 182.984 | 2.6 ± 0.8 |
| | $6_{1,6}$ | 3798.189 | 308.616 | 1.9 ± 0.6 |
| | $7_{0,7}$ | 3810.595 | 403.162 | 2.1 ± 0.6 |
| | $7_{1,6}$ | 3826.241 | 473.918 | 2.4 ± 0.7 |
| | $\langle k_{dep}\rangle = (2.3 \pm 0.7) \times 10^{-9}$ cm$^3$ molecule$^{-1}$ s$^{-1}$ [b] | | | |
| 2,6-lutidine | $2_{2,0}$ | 3702.904 | 109.269 | 2.4 ± 0.7 |
| | $4_{1,3}$ | 3787.510 | 182.984 | 2.9 ± 0.9 |
| | $6_{1,6}$ | 3798.189 | 308.616 | 2.7 ± 0.8 |
| | $7_{0,7}$ | 3810.595 | 403.162 | 2.1 ± 0.6 |
| | $7_{1,6}$ | 3826.241 | 473.918 | 1.7 ± 0.5 |
| | $\langle k_{dep}\rangle = (2.5 \pm 0.7) \times 10^{-9}$ cm$^3$ molecule$^{-1}$ s$^{-1}$ [b] | | | |

[a] Based on data presented in the literature.[25,26] [b] $\langle k_{dep}\rangle$ is a population-weighted average of separate $k_{dep}$ measurements.

$$P_J(\Delta E)\mathrm{d}\Delta E = \frac{4\pi}{\mu}\frac{k_{\mathrm{app}}^J}{k_{\mathrm{col}}} g_{\mathrm{f}}\left(\frac{\mu}{2\pi k_{\mathrm{B}} T_{\mathrm{rel}}}\right)^{3/2} \exp\left(-\frac{\mu g_{\mathrm{f}}^2}{2k_{\mathrm{B}} T_{\mathrm{rel}}}\right)\mathrm{d}\Delta E \quad (8)$$

Here, $k_B$ is Boltzmann's constant, $\mu$ is the reduced mass, and $g_f$ is the final velocity. The energy change $\Delta E$ is based on average initial rotational and translational energies at 298 K. The energy transfer probability curves for 2-picoline and 2,6-lutidine are shown in Figure 8 together with $P(\Delta E)$ for pyrazine.[25,26] The energy transfer probability is shown relative to the experimental collision rate ($k_{app}$) in Figure 8a and relative to the Lennard−Jones collision rate in Figure 8b. Note that $P(\Delta E)$ curves based on the Lennard−Jones collision rate are not normalized to unity probability.

We can determine average energy transfer values $\langle\Delta E\rangle$ from the energy transfer distribution functions using eq 9

$$\langle\Delta E\rangle = \int P(\Delta E)\Delta E \mathrm{d}(\Delta E) \quad (9)$$

It is important to use normalized P($\Delta E$) curves such as in Figure 8a to determine $\langle\Delta E\rangle$ values. The average energy transfer values for pyrazine/HOD, 2-picoline/HOD, and 2,6-lutidine/HOD collisions are very similar: $\langle\Delta E\rangle$ = 554, 601, and 502 cm$^{-1}$ respectively. The similarity of the $\langle\Delta E\rangle$ values comes from the similarity of the HOD(000) translational and rotational distributions. The resulting $\langle\Delta E\rangle$ values correspond to energy transfer on a per collision basis. However, lutidine($E$) is actually quenched faster than pyrazine($E$) or picoline($E$) under similar collision conditions because lutidine has a larger collision rate with HOD. If instead the $P(\Delta E)$ curves are based on the Lennard−Jones collision rate, the average energy transfer values are $\langle\Delta E\rangle$ = 918, 1157, and 1254 cm$^{-1}$ for pyrazine, 2-picoline, and 2,6-lutidine, respectively. This comparison highlights an important subtlety in interpreting collisional quenching results, namely that both the collision rate and the energy transfer distribution affect quenching efficiency. Since the Lennard−Jones model underestimates HOD collision rates, it overestimates the average energy transferred. On the other hand, normalizing $P(\Delta E)$ with the observed collision rate removes effects that are caused by differences in the collision rates. This issue is particularly important for understanding the kinetics of mixtures of gases that have a range of collision rates. An accurate description of energy transfer between ensembles of molecules requires both the $P(\Delta E)$ curve and an accurate collision rate.

The results presented here provide insight into previous reports of unusually large quenching efficiencies due to water collisions both for small molecules with low level of vibrational energy and larger polyatomic molecules with large amounts of vibrational energy.[27,28] For example, $CO_2(01^10)$ is relaxed 100 times faster by collisions with $H_2O$ than with $CO_2$.[29] For aromatic molecules, enhanced quenching by water has been observed in UV absorption,[31,33,61] IR fluorescence,[30,32,35] and thermal lensing[34] experiments that measure energy loss from highly excited molecules. Water is three times more efficient than $CO_2$ at quenching triplet pyrazine ($E$ = 5000 cm$^{-1}$).[62] Singlet state benzene($E$ = 24000 cm$^{-1}$) transfers on average 208 cm$^{-1}$ per collision with $CO_2$ and 373 cm$^{-1}$ per collision with water, based on Lennard−Jones collision rates.[30] In another example, singlet state azulene ($E$ = 24000 cm$^{-1}$) transfers 360 cm$^{-1}$ on average per $CO_2$ collision and 480 cm$^{-1}$ in collisions with water.[61] It is likely that enhanced collision rates contribute to water's ability to quench vibrationally excited molecules.

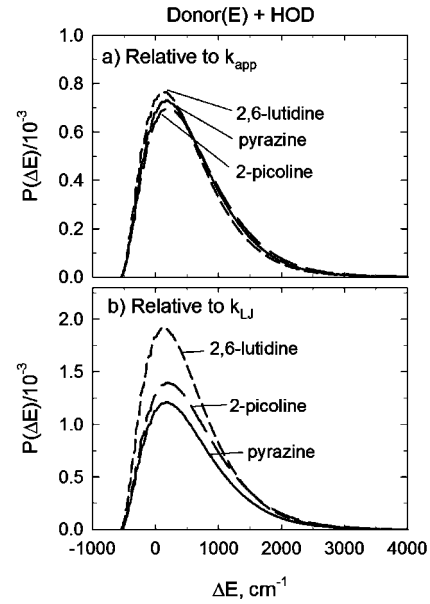


**Figure 8.** Energy transfer probability distribution functions for pyrazine/HOD(solid line), 2-picoline (long dashed line), and 2,6-lutidine (short dashed line) relative to (a) $k_{app}$, the experimentally measured collision rate and (b) the Lennard−Jones collision rate.

What is not known, however, is the extent to which the collision rate leads to enhanced energy transfer values and the extent to which the distribution of exchanged energy is important. The interplay between collision rate and the energy transfer distribution determines the overall effectiveness for removing vibrational energy from highly excited molecules through collisions.

It is interesting that the energy transfer distribution functions for collisions of HOD with pyrazine, picoline, and lutidine are relatively insensitive to the identity of the donor molecule. Full distributions have not been measured for collisions of these donors with $H_2O$ and $CO_2$, but studies on the strong collisions of $H_2O$ and $CO_2$ with these donors show that donor identity and internal energy has a significant effect on the energy distributions of the scattered bath molecules.[4,63−66] These differences have been correlated with changes in the vibrational state density of the donor molecule and interpreted as involving impulsive collisions. It could be that the stronger interaction of HOD with these donors changes the nature of the collisions in such as way as to limit the opportunity to fully explore the available phase space of the highly excited molecules. The idea of limited access to the available phase space of the colliding molecules is at the heart of the Partial Ergodic Collision Theory (PECT) developed by Nordholm and co-workers.[67,68] By reducing the available phase space, PECT is able to reproduce experimental results from KCSI experiments.[69] Developing accurate potential energy surfaces for these donors with HOD and $H_2O$ should provide insight into this possibility.

## Conclusion

This work has investigated the state-resolved relaxation dynamics of highly vibrationally excited 2-picoline and 2,6-lutidine with HOD and made comparisons to previous results on pyrazine with HOD. High resolution transient IR absorption was used to measure the full distribution of scattered HOD(000) molecules. These studies were possible because of new developments for obtaining transient appearance measurements of low energy bath states. Doppler-broadened line profiles, rotational distributions, energy transfer rates, and complete energy transfer

probability distribution functions are reported here. The scattering profiles for HOD are remarkably similar for quenching the three donors in this study. The scattered HOD(000) molecules have relatively small amounts of rotational and translational energy. No evidence was seen for vibrational excitation of HOD. The full energy transfer distribution functions show that the average energy transfer is $<\Delta E> \sim 550$ $cm^{-1}$ for these collision pairs. The overall energy transfer rates show differences for these donors and have the order of 2,6-lutidine > 2-picoline> pyrazine.

Molecular collision rates were directly determined from summing over state-specific rates for appearance of energy transfer products. The observed collision rates for the three donors with HOD are each larger than the Lennard−Jones collision rate. Pyrazine/HOD collisions have a rate that is ∼1.7 times the Lennard−Jones rate. For 2-picoline/HOD, the collision rate is ∼2.5 times the Lennard−Jones collision rate. For 2,6-lutidine/HOD, this ratio is ∼3.2. The enhancements in collision rates are likely due to hydrogen bonding interactions, internal energy of the highly excited donors or both. Studies of this type provide an important benchmark for developing more accurate models of collisional energy transfer and collision rates.

## References and Notes


(1) Orchard, S. W.; Ramsden, J. *Int. J. Chem. Kinet.* **1982**, *14*, 43.
(2) Rizzo, T. R.; Crim, F. F. *J. Chem. Phys.* **1982**, *76*, 2754.
(3) Larson, C. W.; Rabinovitch, B. S. *J. Chem. Phys.* **1969**, *51*, 2293.
(4) Elioff, M. S.; Fang, M.; Mullin, A. S. *J. Chem. Phys.* **2001**, *115*, 6990.
(5) Fraelich, M.; Elioff, M. S.; Mullin, A. S. *J. Phys. Chem. A* **1998**, *102*, 9761.
(6) Chan, S. C.; Rabinovitch, B. S.; Bryant, J. T.; Spicer, L. D.; Fujimoto, T.; Lin, Y. N.; Pavlou, S. P. *J. Phys. Chem.* **1970**, *74*, 3160.
(7) Lendvay, G.; Schatz, G. C. *J. Phys. Chem.* **1992**, *96*, 3752.
(8) Utz, A. L.; Tobiason, J. D.; Carrasquillo, E.; Fritz, M. D.; Crim, F. F. *J. Chem. Phys.* **1992**, *97*, 389.
(9) Troe, J. *J. Chem. Phys.* **1977**, *66*, 4745.
(10) Troe, J. *J. Chem. Phys.* **1977**, *66*, 4758.
(11) Snavely, D. L.; Zare, R. N.; Miller, J. A.; Chandler, D. W. *J. Phys. Chem.* **1986**, *90*, 3544.
(12) Barrett, J. C. *J. Chem. Phys.* **2007**, *126*, 074312.
(13) Barrett, J. C. *J. Chem. Phys.* **2002**, *116*, 8856.
(14) Ford, I. J. *Proc. Inst. Mech. Eng. C, J. Mech. Eng. Sci.* **2004**, *218*, 883.
(15) Oxtoby, D. W. *J. Phys.: Condens. Matter* **1992**, *4*, 7627.
(16) Xue, B.; Han, J.; Dai, H.-L. *Phys. Rev. Lett.* **2000**, *84*, 2606.
(17) Durant, J. L.; Kaufman, F. *Chem. Phys. Lett.* **1987**, *142*, 246.
(18) Hinchen, J. J.; Hobbs, R. H. *J. Chem. Phys.* **1976**, *65*, 2732.
(19) Lim, K. F. *Quantum Chem. Program Exchange Bull.* **1994**, *14*, 3.
(20) Mourits, F. M.; Rummens, F. H. A. *Can. J. Chem.* **1977**, *55*, 3007.
(21) Whetton, N. T.; Lawrance, W. D. *J. Phys. Chem.* **1992**, *96*, 3717.
(22) Tasic, U. S.; Parmenter, C. S. *J. Phys. Chem. B* **2004**, *108*, 10325.
(23) Michael, J. V.; Su, M. C.; Sutherland, J. W.; Carroll, J. J.; Wagner, A. F. *J. Phys. Chem. A* **2002**, *106*, 5297.
(24) Hirschfelder, J. O.; Curtiss, C. F.; Bird, R. B. *Molecular Theory of Gases and Liquids*; John Wiley and Sons: New York, 1964.
(25) Havey, D. K.; Liu, Q.; Li, Z.; Elioff, M.; Fang, M.; Neudel, J.; Mullin, A. S. *J. Phys. Chem. A* **2007**, *111*, 2458.
(26) Havey, D. K.; Liu, Q.; Li, Z.; Elioff, M.; Mullin, A. S. *J. Phys. Chem. A* **2007**, *111*, 13321.
(27) Yardley, J. T. *Introduction to Molecular Energy Transfer*; Academic Press Inc.: New York, 1980.
(28) Cottrell, T. L.; McCoubrey, J. C. *Molecular Energy Transfer in Gases*; Butterworths: London, 1961.
(29) Keeton, R. G.; Bass, H. E. *J. Acoust. Soc. Am.* **1976**, *60*, 78.
(30) Barker, J. R.; Toselli, B. M. *Int. Rev. Phys. Chem.* **1993**, *12*, 305.
(31) Heymann, M.; Hippler, H.; Plach, H. J.; Troe, J. *J. Chem. Phys.* **1987**, *87*, 3867.
(32) Rossi, M. J.; Pladziewicz, J. R.; Barker, J. R. *J. Chem. Phys.* **1983**, *78*, 6695.
(33) Hippler, H.; Troe, J. *Advances in Gas-Phase Photochemistry and Kinetics: Bimolecular Collisions*; Ashfold, M. N. R., Baggott, J. E., Eds.; Royal Society of Chemistry: London, 1989.
(34) Toselli, B. M.; Walunas, T. L.; Barker, J. R. *J. Chem. Phys.* **1990**, *92*, 4793.
(35) Yerram, M. L.; Brenner, J. D.; King, K. D.; Barker, J. R. *J. Phys. Chem.* **1990**, *94*, 6341.
(36) Elioff, M. S.; Sansom, R. L.; Mullin, A. S. *J. Phys. Chem. A* **2000**, *104*, 10304.
(37) Elioff, M. S.; Fraelich, M.; Sansom, R. L.; Mullin, A. S. *J. Chem. Phys.* **1999**, *111*, 3517.
(38) Lenzer, T.; Luther, K.; Reihs, K.; Symonds, A. C. *J. Chem. Phys.* **2000**, *112*, 4090.
(39) Hold, U.; Lenzer, T.; Luther, K.; Symonds, A. C. *J. Chem. Phys.* **2003**, *119*, 11192.
(40) Luther, K.; Reihs, K. *Ber. Bunsen-Ges. Phys. Chem. Chem. Phys.* **1988**, *92*, 442.
(41) Grigoleit, U.; Lenzer, T.; Luther, K. *Z. Phys. Chem. (Muenchen, Ger.)* **2000**, *214*, 1065.
(42) Luther, K.; Reihs, K. *Ber. Bunsen-Ges. Phys. Chem. Chem. Phys.* **1988**, *92*, 442.
(43) Lenzer, T.; Luther, K.; Reihs, K.; Symonds, A. C. *J. Chem. Phys.* **2000**, *112*, 4090.
(44) Hold, U.; Lenzer, T.; Luther, K.; Reihs, K.; Symonds, A. C. *J. Chem. Phys.* **2000**, *112*, 4076.
(45) Hold, U.; Lenzer, T.; Luther, K.; Symonds, A. C. *J. Chem. Phys.* **2003**, *119*, 11192.
(46) Liu, C. L.; Hsu, H. C.; Lyu, J. J.; Ni, C. K. *J. Chem. Phys.* **2005**, *123*, 131102.
(47) Liu, C. L.; Hsu, H. C.; Lyu, J. J.; Ni, C. K. *J. Chem. Phys.* **2006**, *124*, 054302.
(48) Liu, C. L.; Hsu, H. C.; Ni, C. K. *Phys. Chem. Chem. Phys.* **2005**, *7*, 2151.
(49) Sushida, K.; Yamazaki, I.; Baba, H. *Oyo Denki Kenkyusho Hokoku* **1980**, *32*, 36.
(50) Pyper, J. W.; Christensen, L. D. *J. Chem. Phys.* **1975**, *62*, 2596.
(51) Elioff, M. S.; Fang, M.; Mullin, A. S. *J. Chem. Phys.* **2002**, *117*, 6880.
(52) Caminati, W.; Favero, L. B.; Favero, P. G.; Maris, A.; Melandri, S. *Angew. Chem., Int. Ed.* **1998**, *37*, 792.
(53) Danten, Y.; Tassaing, T.; Besnard, M. *J. Phys. Chem. A* **1999**, *103*, 3530.
(54) Clarkson, J. R.; Baquero, E.; Shubert, V. A.; Myshakin, E. M.; Jordan, K. D.; Zwier, T. S. *Science* **2005**, *307*, 1443.
(55) Liu, Q.; Havey, D. K.; Mullin, A. S. *J. Phys. Chem. A* **2008**, *112*, 9509.
(56) Lide, D. R. *CRC Handbook of Chemistry and Physics*; CRC Press Inc.: Boca Raton, FL, 2004−2005.
(57) Diken, E. G.; Shin, J. W.; Price, E. A.; Johnson, M. A. *Chem. Phys. Lett.* **2004**, *387*, 17.
(58) Macomber, R. *Organic Chemistry*; University Science Books: New York, 1996; Vol. II.
(59) Pankratov, A. N. *Heteroat. Chem.* **2002**, *13*, 229.
(60) Michaels, C. A.; Flynn, G. W. *J. Chem. Phys.* **1997**, *106*, 3558.
(61) Hippler, H.; Otto, B.; Troe, J. *Phys. Chem. Chem. Phys.* **1989**, *93*, 428.
(62) McDowell, D. R.; Wu, F.; Weisman, R. B. *J. Chem. Phys.* **1998**, *108*, 9404.
(63) Liu, Q.; Du, J.; Havey, D. K.; Li, Z.; Miller, E. M.; Mullin, A. S. *J. Phys. Chem. A* **2007**, *111*, 4073.
(64) Miller, E. M.; Murat, L.; Bennette, N.; Hayes, M.; Mullin, A. S. *J. Phys. Chem. A* **2006**, *110*, 3266.
(65) Park, J.; Shum, L.; Lemoff, A. S.; Werner, K.; Mullin, A. S. *J. Chem. Phys.* **2002**, *117*, 5221.
(66) Yuan, L. W.; Du, J.; Mullin, A. S. *J. Chem. Phys.* **2008**, *129*, 014303.
(67) Nilsson, D.; Nordholm, S. *J. Chem. Phys.* **2003**, *119*, 11212.
(68) Nilsson, D.; Nordholm, S. *J. Phys. Chem. A* **2006**, *110*, 3289.
(69) Lenzer, T.; Luther, K.; Nilsson, D.; Nordholm, S. *J. Phys. Chem. B* **2005**, *109*, 8325.
(70) Bevilacqua, T. J.; Weisman, R. B. *J. Chem. Phys.* **1993**, *98*, 6316.
(71) Mcquarrie, D. A. *Statistical Mechanics*; University Science Books: New York, 2000.


JP811077P